UCRL-JC-132242
PREPRINT

A Model For Simulating Airflow and Pollutant Dispersion around Buildings

Stevens T. Chan
Robert L. Lee

This paper was prepared for submittal to
AIR POLLUTION 99
27–29 July 1999
San Francisco, CA

February 1999

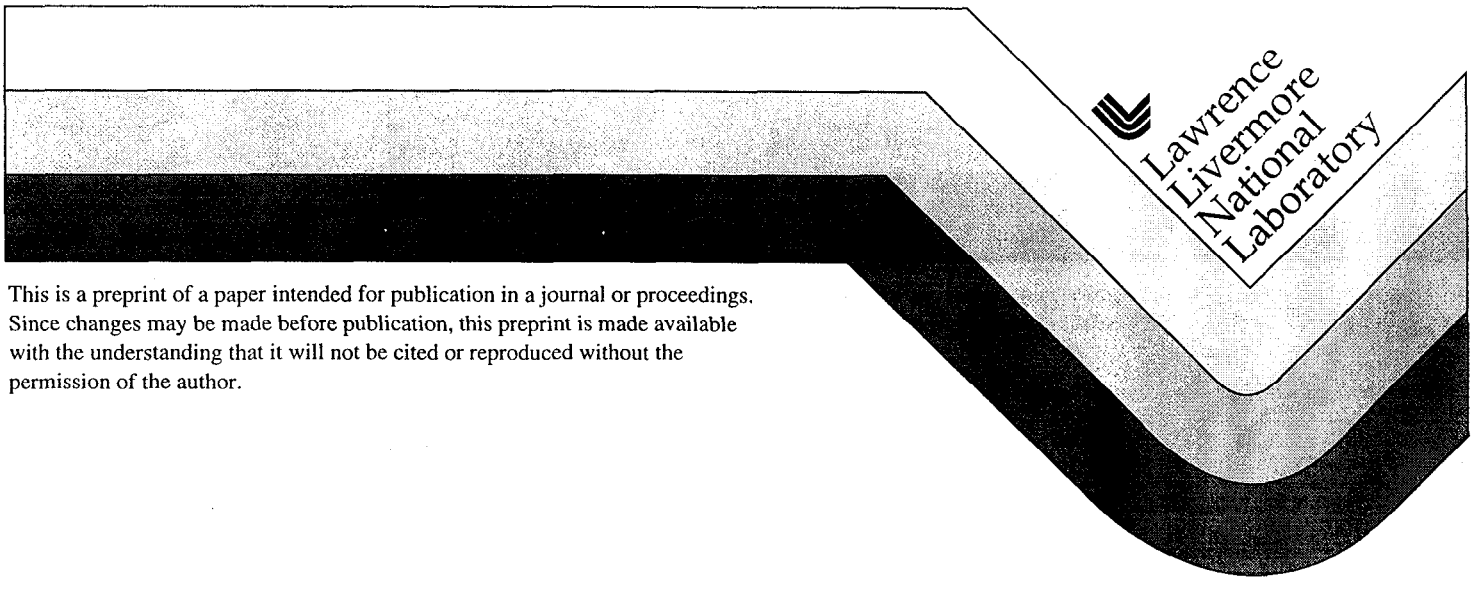

A model for simulating airflow and pollutant dispersion around buildings

S.T. Chan[1] and R.L. Lee[2]
[1] *Lawrence Livermore National Laboratory, P.O. Box 808, L-103, Livermore, CA 94551, e-mail: schan@llnl.gov*
[2] *Lawrence Livermore National Laboratory, P.O. Box 808, L-103, Livermore, CA 94551, e-mail: lee34@llnl.gov*

Abstract

A three-dimensional, numerical model for simulating airflow and pollutant dispersion around buildings is described. The model is based on an innovative finite element approach and fully implicit time integration techniques. Linear and nonlinear eddy viscosity/diffusivity submodels are provided for turbulence parameterization. Model predictions for the flow-field and dispersion patterns around a surface-mounted cube are compared with measured data from laboratory experiments.

1. Introduction

The prediction of atmospheric flow and pollutant dispersion in an urban area is difficult due to the presence of buildings and numerous surface-mounted obstacles. Individual buildings exhibit significant geometrical variations with building wakes from adjacent buildings interfering and altering the trajectory of street level plumes. We are developing numerical models for predicting airflow and pollutant dispersal on building-scales from a single building to multi-building complexes. These models will be used as assessment tools for emergency response planning and could be extended to provide input for real-time responses.

The key computational model we are developing is called FEM3CB, with its primary applications intended for predicting the dispersion of chem-bio agents around buildings. The model is based on the FEM3C model (Chan[1]), which has been developed and validated for simulating the dispersion of heavier-than-air gases in the atmosphere (see, for example, Chan, *et al.*[2]; Chan[3]). FEM3C solves

the three-dimensional, time-dependent, incompressible Navier-stokes equations with turbulence represented via a similarity-theory based K submodel or a $k-\varepsilon$ transport equation submodel.

The initial version of FEM3CB has been greatly improved over FEM3C in the areas of computational speed and physics. We have implemented a new pressure solver, an implicit time-integration algorithm, and a multi-processing capability. As a result, we have gained a 20-fold reduction in computational time and are able to perform a typical dispersion simulation in a few hours on a DEC Alpha computer. New physics added to the code include a first-order ultraviolet radiation decay submodel for biological agents and the treatment of surface deposition and gravitational settling for aerosols.

We are currently implementing other relevant physics into FEM3CB, including canopy and vegetation effects, building shadowing effects, and a surface energy budget submodel for ground heating effects. In addition, we are investigating the use of a three-equation nonlinear eddy viscosity submodel and a large eddy simulation (LES) submodel for more accurate turbulence parameterization. Furthermore, we are developing a massively parallelized version to enable us to further improve the model's computational speed and to expand the number of buildings in future simulations.

In this paper, the main features of our present model are briefly described, a model evaluation study is conducted, using laboratory data for flow and dispersion around a cube, and a few concluding remarks are made.

2. Numerical model

2.1 Governing Equations

The following three-dimensional Reynolds-averaged conservation equations, coupled with a turbulence submodel, are solved by FEM3CB. For brevity, the equations are presented for species in vapor phase only, although FEM3CB also treats aerosols. The equations, written in Cartesian tensor form, are:

$$\frac{\partial}{\partial t}(\rho u_i)+\rho u_j\frac{\partial u_i}{\partial x_j}=-\frac{\partial p}{\partial x_i}+\frac{\partial}{\partial x_j}(-\rho\overline{u_i'u_j'})+(\rho-\rho_h)g_i \quad , \tag{1}$$

$$\frac{\partial}{\partial x_j}(\rho u_j)=0 \quad , \tag{2}$$

$$\frac{\partial\theta}{\partial t}+u_j\frac{\partial\theta}{\partial x_j}=\frac{1}{\rho C_p}\frac{\partial}{\partial x_j}(-\rho C_p\overline{u_j'\theta'})+\frac{C_{pv}-C_{pa}}{\rho C_p}(-\rho\overline{u_j'q_v'})\frac{\partial\theta}{\partial x_j} \quad , \tag{3}$$

$$\frac{\partial}{\partial t}(\rho q_v)+\rho u_j\frac{\partial q_v}{\partial x_j}=\frac{\partial}{\partial x_j}(-\rho\overline{u_j'q_v'})+\lambda\left(\rho q_v\right)+w_s\frac{\partial(\rho q_v)}{\partial x_3} \quad , \tag{4}$$

$$\rho = \frac{PM_a}{RT\left[1+\left(\frac{M_a}{M_v}-1\right)q_v\right]} \quad , \tag{5}$$

and

$$C_p = C_{pv}q_v + (1-q_v)C_{pa} \quad . \tag{6}$$

In the above equations, u_i is the i-th component of the mean velocity, θ is the potential temperature deviation from a base state (θ_0), q_v is the mass fraction of species, ρ is the mixture density, p is the pressure deviation from a hydrostatic pressure field (p_h), ρ_h is the density field corresponding to p_h, g_i is the gravitational acceleration, C_p, C_{pa}, and C_{pv} are the specific heats of the mixture, air, and species. In the species equation, λ is the decay (or rate) constant and w_s is the absolute value of gravitational settling velocity for aerosols.

2.2 Turbulence Submodels

In addition to a K-theory turbulence submodel (Chan, *et al.*[2]), we also implemented a slightly modified version of the buoyancy-extended $k-\varepsilon$ turbulence submodel developed by Haroutunian[4]. The salient features of our $k-\varepsilon$ submodel are given below. More details can be found in Chan[1].

The turbulent fluxes are modeled as:

$$-\rho\overline{u_i'u_j'} = \rho K_{ijlm}\left(\frac{\partial u_\ell}{\partial x_m}+\frac{\partial u_m}{\partial x_\ell}\right)-\frac{2}{3}\rho k\delta_{ij} \quad , \tag{7}$$

$$-\rho\overline{u_i'\theta'} = \rho K_{ij}^{\theta}\frac{\partial\theta}{\partial x_j} \quad , \quad -\rho\overline{u_i'q_v'} = \rho K_{ij}^{c}\frac{\partial q_v}{\partial x_j} \quad , \tag{8}$$

where k_{ijlm}, k_{ij}^{θ}, k_{ij}^{c} are the eddy viscosity/diffusivity tensors for momentum, energy, and species, respectively. The diffusion tensors are approximated as:

$$K_{ijlm} \longrightarrow C_\mu\frac{k^2}{\varepsilon}\begin{Bmatrix} 1 & \beta_H & 1 \\ \beta_H & 1 & 1 \\ 1 & 1 & 1 \end{Bmatrix} \quad , \quad P_{rt}K_{ij}^{\theta} = P_{rt}K_{ij}^{c} = C_\mu\frac{k^2}{\varepsilon}\begin{Bmatrix} \beta_H & 0 & 0 \\ 0 & \beta_H & 0 \\ 0 & 0 & 1 \end{Bmatrix} \quad , \tag{9}$$

wherein P_{rt} is the turbulent Prandtl number determined by the flux Richardson number (see Ueda *et al.*[5]), $C_\mu = 0.09$, and β_H is an input parameter.

The variables k and ε in Eq. (9) are obtained from solving the following transport equations,

$$\frac{\partial}{\partial t}(\rho k)+\rho u_j\frac{\partial k}{\partial x_j}=\frac{\partial}{\partial x_i}\left(\rho K_{ij}^{k}\frac{\partial k}{\partial x_j}\right)+s+b-\rho\varepsilon\ , \tag{10}$$

$$\frac{\partial}{\partial t}(\rho\varepsilon)+\rho u_j\frac{\partial \varepsilon}{\partial x_j}=\frac{\partial}{\partial x_i}\left(\rho K_{ij}^{\varepsilon}\frac{\partial \varepsilon}{\partial x_j}\right)+C_1\left(\frac{\varepsilon}{k}\right)s$$
$$+C_1\left(1-C_3\right)\left(\frac{\varepsilon}{k}\right)b-C_2\rho\left(\frac{\varepsilon^2}{k}\right), \tag{11}$$

wherein K_{ij}^{k} and K_{ij}^{ε} are the eddy diffusivity tensors for k and ε respectively. The model constants are: $C_1=1.44$, $C_2=1.92$, and $C_3=-0.8$ and 2.15 for the unstable and stable regimes respectively.

Also implemented in our code is a nonlinear eddy viscosity turbulence submodel developed by Suga[6]. This 3-equation turbulence submodel has many desirable properties, including anisotropy, a cubic constitutive law, and no need for wall functions. It suffers from none of the maladies that normally afflict the commonly used $k-\varepsilon$ turbulence submodel. Additionally, since the model has been derived from the Reynolds stress closure models, it retains many of their attributes—but at a significantly reduced computational cost. We have implemented and briefly tested the submodel in another time-dependent Navier-Stokes solver and obtained highly encouraging results in a simulation of the flow pass an automobile-like body (Gresho and Chan[7]).

The crux of the submodel involves the following three fairly complex, coupled equations, with details available in Suga[6], Chan and Gresho[7]:

$$\frac{\partial k}{\partial t}+u_j\frac{\partial k}{\partial x_j}=\frac{\partial}{\partial x_i}\left[\left(\nu\delta_{ij}+0.22f_g\overline{u_i'u_j'}\frac{k}{\bar{\varepsilon}}\right)\frac{\partial k}{\partial x_j}\right]+P_K-\varepsilon\ , \tag{12}$$

$$\frac{\partial \bar{\varepsilon}}{\partial t}+u_j\frac{\partial \bar{\varepsilon}}{\partial x_j}=\frac{\partial}{\partial x_i}\left[\left(\nu\delta_{ij}+0.18f_g\overline{u_i'u_j'}\frac{k}{\bar{\varepsilon}}\right)\frac{\partial \bar{\varepsilon}}{\partial x_j}\right]$$
$$+\left(1.2P_K-C_\varepsilon\bar{\varepsilon}\right)\frac{\bar{\varepsilon}}{k}+P_\varepsilon\ , \tag{13}$$

$$\frac{\partial A_2}{\partial t}+u_j\frac{\partial A_2}{\partial x_j}=\frac{\partial}{\partial x_i}\left[\left(\nu\delta_{ij}+0.22f_g\overline{u_i'u_j'}\frac{k}{\bar{\varepsilon}}\right)\frac{\partial A_2}{\partial x_j}\right]$$
$$+\frac{a_{ij}}{k}\left[P_{ij}-\varepsilon_{ij}+\phi_{ij}\right]-\frac{2A_2}{k}P_K. \tag{14}$$

In the above equations, k is the turbulent kinetic energy, $\bar{\varepsilon}$ is the isotropic dissipation rate, and A_2 is the second invariant of the dimensionless anisotropic Reynolds stress tensor $\left(A_2 = a_{ij}a_{ij}\right)$.

The Reynolds stresses are, in turn, defined by a cubic constitutive relationship

$$\begin{aligned}\overline{u_i'u_j'} = {} & \frac{2}{3}k\delta_{ij} - \nu_T S_{ij} + \frac{\nu_T k}{\bar{\varepsilon}}\Big\{c_1(S_{ik}S_{kj} - \frac{1}{3}S_{k\ell}S_{k\ell}\delta_{ij}) \\ & + c_2\left(\Omega_{ik}S_{kj} + \Omega_{jk}S_{ki}\right) + c_3(\Omega_{ik}\Omega_{jk} - \frac{1}{3}\Omega_{\ell k}\Omega_{\ell k}\delta_{ij}) \\ & + \frac{k}{\bar{\varepsilon}}\Big[c_4\left(S_{k\ell}\Omega_{\ell j} + S_{kj}\Omega_{\ell i}\right)S_{k\ell} + c_5 S_{ij}S_{k\ell}S_{k\ell}\Big] + c_6 S_{ij}\Omega_{k\ell}\Omega_{k\ell}\Big\}\,, \end{aligned} \tag{15}$$

in which S_{ij} is the mean strain rate tensor and Ω_{ij} is the mean rotation tensor.

The isotropic turbulent eddy viscosity is defined as

$$\nu_t = c_\mu f_\mu k^2/\bar{\varepsilon} \tag{16}$$

in which c_μ is a turbulent viscosity parameter and f_μ is a wall damping function.

2.3 Spatial Discretization and Time Integration

The above set of equations are firstly discretized in space by the Galerkin finite element method, with piecewise constant representation for pressure and trilinear approximations for other field variables to obtain a coupled system of nonlinear first-order ordinary differential equations (ODEs). The discretized systems of equations are then solved to provide the transient solutions for all the field variables.

In order to solve cost-effectively large three-dimensional problems, we employ the fully implicit projection method developed by Gresho and Chan[7]. With the method, the coupled system of equations are segregated and solved sequentially for each of the field variables, via either a direct method or an efficient iterative solver. A brief summary of the method is as follows:

(1) Given a divergence-free velocity and its corresponding pressure fields, compute an intermediate velocity field via an implicit time-stepping scheme such as the backward Euler method or the trapezoide rule,
(2) Project the intermediate velocity to a divergence-free subspace via (a) solving a consistently derived pressure Poisson equation for the pressure increment, and (b) updating the velocity field,

(3) Solve sequentially the remaining systems of ODEs for temperature, concentration, and turbulence variables via, again, an implicit time-stepping scheme,
(4) Advance time and go back to (1).

3. Results and discussions

In this example, the FEM3CB model with the $k-\varepsilon$ turbulence submodel was used to calculate the flow-field and dispersion pattern around a surface-mounted cube in a channel with a fully developed turbulent approach flow. The height of the cube (H) is 1.0 and the channel height is twice that of the cube. The mean flow is neutrally stable and has a Reynolds number of 40,000, based on the bulk velocity *(U=0.6)* and the cube height. The cube is centered at 3.5H from the inlet plane, 3H from the lateral boundary, and 6.5H to the downwind exit plane. In the dispersion simulation, an area-source is placed on the ground at 0.25H behind the cube.

Recognizing the symmetric property, we simulated only one-half of the problem, with a graded mesh consisting of $37 \times 36 \times 98$ (vertical $\times$ crosswind $\times$ downwind) grid points. Sample results are presented and compared with laboratory data in the following figures.

Depicted in Fig. 1 are the predicted flow-field and dispersion pattern on the vertical plane of symmetry and the ground surface. The main features of the flow-field include the separations at upstream, on the roof and the two sides, the primary recirculation zone in the wake and a pair of counter-rotating vortices on the horizontal plane. The predicted reattachment length is 2.85 versus 1.61 measured by Martinuzzi and Tropea[8]. Due to the complex flow-field, the plume is lofted, entrained into the sides, and becomes bifurcated in the wake.

In Figs. 2 and 3, the predicted turbulent kinetic energy and velocity profiles are compared with the data of Martinuzzi and Tropea[8]. The agreement between model predictions and data for locations near the cube is good in general; however, the agreement greatly deteriorates at locations further away from the cube. Similar disagreement was reported by Lakehal and Lodi[9] with computer codes using variants of $k-\varepsilon$ turbulence submodels.

In the final figure, the predicted normalized concentrations ($\chi = C^* U^* H^2 / Q$, Q being the source emission rate) are compared with the measured data reported in Zhang, *et al.*[10] The agreement is reasonable, with roughly a factor of two overprediction for downwind concentrations and a much narrower plume width. Our predictions are very consistent with the $k-\varepsilon$ model results reported by Zhang, *et al.*[10]

4. Conclusions

We have presented and demonstrated a numerical model for predicting the flow-field and dispersion pattern around a surfaced-mounted cube. Results from the present study using the $k-\varepsilon$ turbulence submodel suggest that, in order to model airflow and dispersion around buildings accurately, more advanced turbulence parameterization is necessary. Deficiencies of the $k-\varepsilon$ turbulence submodel include the linear stress-strain law, isotropic turbulence assumption, and the use of wall functions. For a balance between model sophistication and cost-effectiveness, the nonlinear eddy viscosity and LES submodels are potentially viable alternatives. We are currently testing the former submodel and results will be reported at the conference.

References

1. Chan, S., FEM3C—An improved three-dimensional heavy-gas dispersion model: User's Manual, UCRL-MA-116567 Rev. 1, Lawrence Livermore National Laboratory, Livermore, CA, 1994.
2. Chan, S.T., Ermak, D.L., and Morris, L.K., FEM3 model simulations of selected Thorney Island Phase I Trials. *J. Haz. Mat.*, **16**, 267–292, 1987.
3. Chan, S.T., Numerical simulations of LNG vapor dispersion from a fenced storage area. *J. Haz. Mat.*, **30**, 195–224, 1992.
4. Haroutunian, V., A time-dependent finite element model for atmospheric dispersion of gases heavier than air, Ph.D. Dissertation, UMIST, U.K, 1987.
5. Ueda, H., S. Mitsumoto, and S. Komori, Buoyancy effects on the turbulent transport processes in the lower atmosphere. *Quart. J.R. Met. Soc.*, **107**, 561–578, 1981.
6. Suga, K., Development and application of a nonlinear eddy viscosity model sensitized to stress and strain invariants. Ph.D. thesis, UMIST, Manchester, UK, 1995.
7. Gresho, P. and S. Chan, Projection 2 goes turbulent—and fully implicit, *Int. J. Comp. Fluid Dyn.*, **9**, 249–272, 1998.
8. Martinuzzi, R. and C. Tropea, The flow around surface-mounted, prismatic obstacles placed in a fully developed channel flow, *J. Fluids Eng.*, **115**, 85–92, 1993.
9. Lakehal, D. and W. Rodi, Calculation of the flow past a surface-mounted cube with two-layer turbulence models, *J. Wind Eng. Ind. Aerodyn.*, **67&68**, 65–78, 1997.
10. Zhang, Y., S. Arya, and W. Snyder, A comparison of numerical and physical modeling of stable atmospheric flow and dispersion around a cubical building, *Atm.Env.* **30**, 1327–1345, 1996.

Acknowledgments

This work was performed under the auspices of the U.S. Department of Energy by Lawrence Livermore National Laboratory under contract number W-7405-ENG-48.

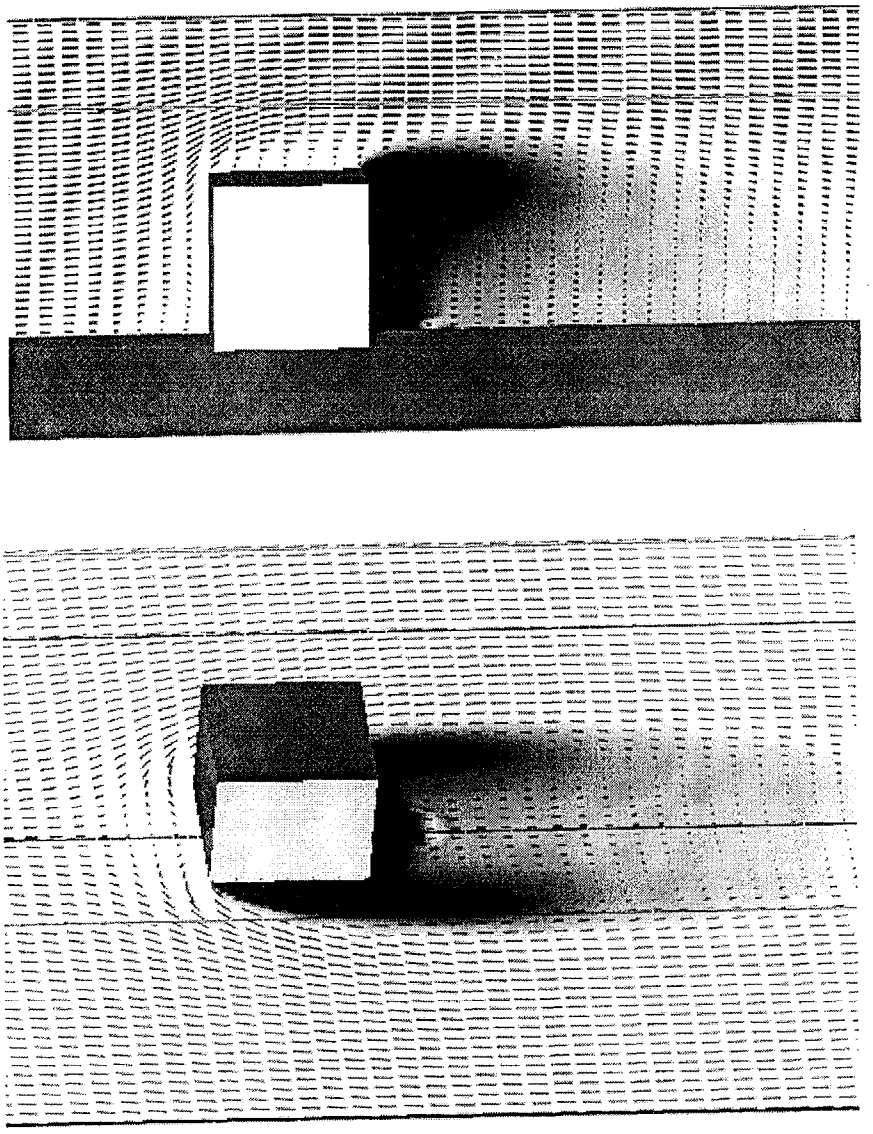

Figure 1: Predicted velocity projection and dispersion pattern near the cube on:
(a) the vertical plane of symmetry, and
(b) the ground surface.

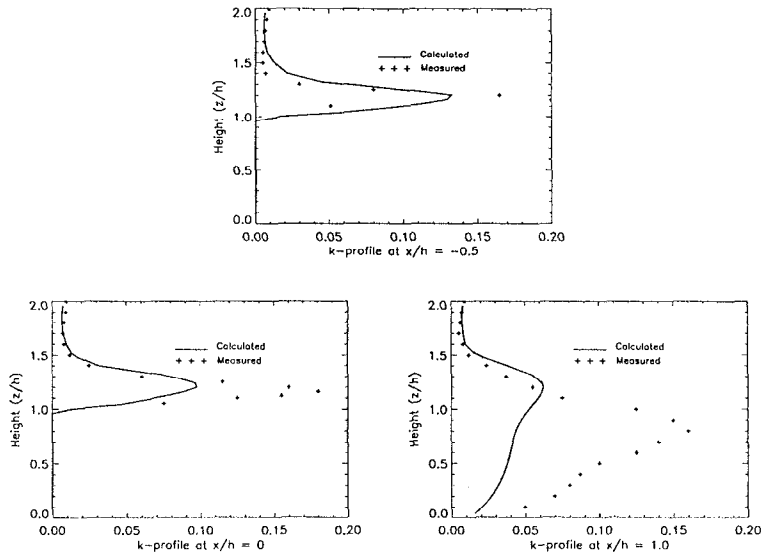

Figure 2: Predicted versus measured k-profiles along three vertical lines on the plane of symmetry. x is measured from the rear surface of the cube.

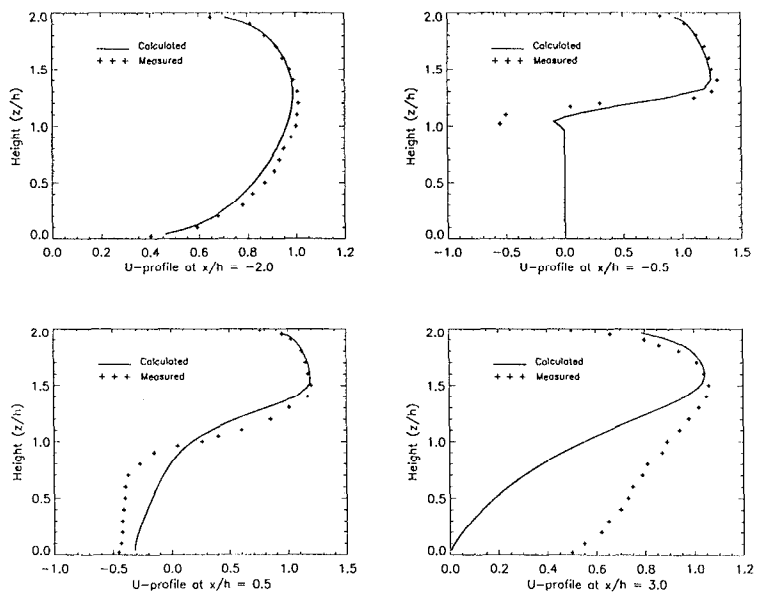

Figure 3: Predicted versus measured U-profiles along four vertical lines on the plane of symmetry. x is measured from the rear surface of the cube.

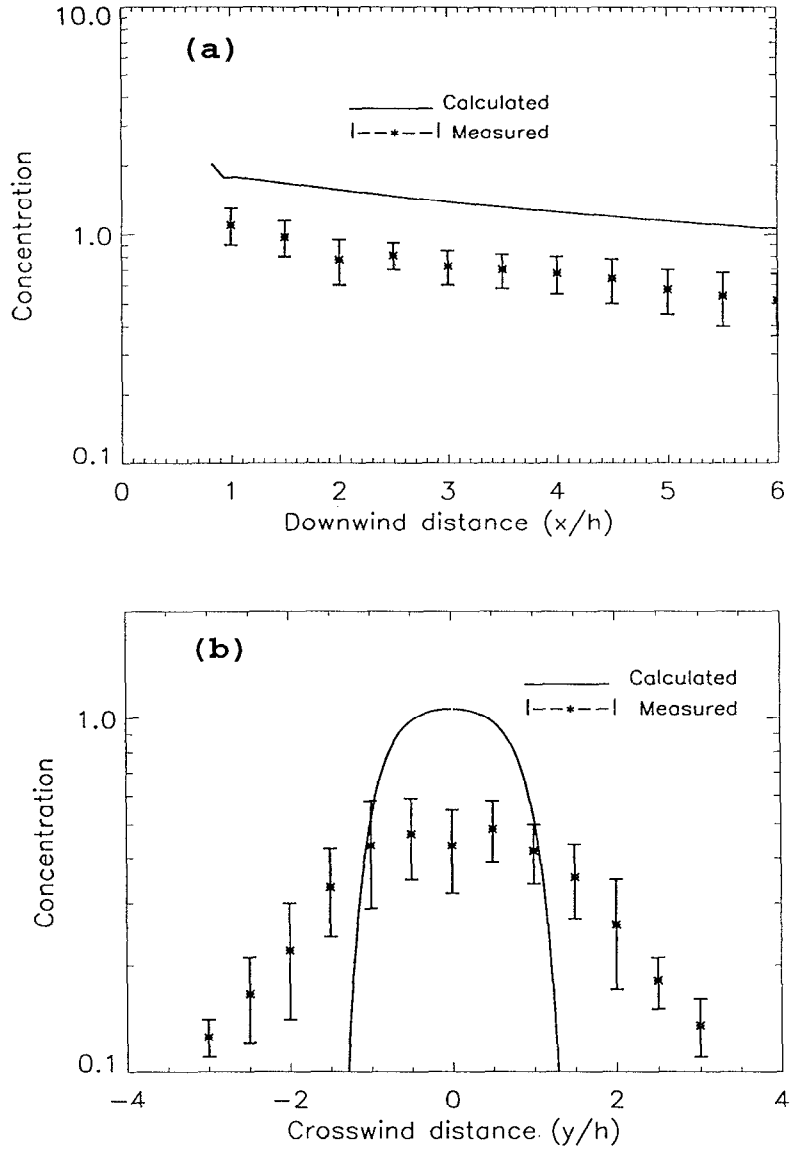

Figure 4: Predicted versus measured normalized concentrations ($\chi = C \cdot U \cdot H^2 / Q$):
(a) downwind ground-level concentration, and
(b) crosswind ground-level concentration.